Toward Complete Path Planning for Planar 3R-Manipulators Among Point Obstacles

Guanfeng Liu[1], J.C. Trinkle[1] and R.J. Milgram[2]

[1] Department of Computer Science, Rensselaer Polytechnic Institute, Troy, NY 12180, USA liugf,trink@cs.rpi.edu
[2] Department of Mathematics, Stanford University, Stanford, CA 94305, USA milgram@math.stanford.edu

1 Abstract

The problem of a planning collision-free motion of a planar 3R-manipulator among point obstacles is studied using techniques from topology and homology. By completely characterizing the set of singular configurations (the points in configuration space corresponding to an intersection of the chain with itself or a point obstacle), the complementary space, the free space, is also completely characterized. This characterization dictates an exact, complete, motion planning algorithm that builds on the authors' algorithm developed for 2R-manipulators [9]. Results obtained with a preliminary version of the algorithm are given.

2 Introduction

For almost two decades, robotics researchers have worked to develop theories and algorithms for important motion planning problems such as manufacturing automation, dexterous manipulation by multifingered hands, multivehicle coordination, robotic surgery, protein folding prediction, and space exploration. A broad overview of these problems and the corresponding planning methods can be found in the survey paper by Hwang and Ahuja [5] and in the text of Latombe [8]. The related history is briefly summarized below.

Lozano-Pérez [11] was among the first to propose the configuration space, C-space, setting for path planning. It is the space of all possible configurations of the robot, ignoring constraints such as joint limits and collisions. In C-space, a point defines a particular pose of the robot and a continuous curve represents a motion of the robot. C-space is normally partitioned into two mutually exclusive subsets:

1. **C-obstacle** - the set of configurations for which the robot's would overlap with one or more obstacles in the workspace.

2. **C-free** - the complement in C-space of the closure of C-obstacle.

C-space transforms the motion planning problem into the problem of finding a continuous curve in C-free that connects given initial and final configurations of the robot.

Since the work of Lozano-Pérez, research in motion planning has branched in two primary directions: (i) the search for exact, complete[3] algorithms; (ii) the development of fast, approximate algorithms. Exact and complete algorithms are necessarily based on an exact representation of C-free. Efforts in the first direction began with Schwartz and Sharir [13, 12], who proposed to decompose C-free into a collection of non-overlapping cells and to represent cell connectivity using a graph. With this representation, the path existence question can be answered by graph search. The problem with this approach is that it relies on a cylindrical algebraic decomposition of C-free, and unfortunately, the complexity of the decomposition is doubly exponential in the dimension of C-space. Canny's roadmap algorithm [1] is the most efficient complete algorithm for general motion planning problems. This algorithm iteratively seeks a low-dimensional retraction of C-free by employing the techniques from differential topology. The complexity is only singly exponential in the dimension of C-space, and thus represents a major improvement. However, because of its intricacy, no full implementation of this algorithm exists.

To side-step the difficulties discussed above, researchers have developed exact algorithms for less general systems (e.g., [4]) and approximate hybrid algorithms combining the techniques of cell decomposition, retraction, and/or potential fields with various heuristics (*e.g,* [3, 2]). Most effort has been spent on the approximate methods, the most popular of which are variants of the probabilistic roadmap method (PRM) proposed by Kavraki *et al.* [7]. These algorithms use pseudo-random sampling and collision detection algorithms to construct a graph that approximates C-free well enough to answer planning queries quickly. These algorithms are *probabilistically complete*, which means that if one samples long enough (with truly random sampling), a path will be found if one exists. However, if a path does not exist, these algorithms cannot determine this fact definitively. In general, while PRMs are effective in many cases, they can be quite ineffective when the valid portion of C-space contains narrow passages. Further, the fact that, in the worst case, C-free contains a number of components exponential in the dimension of C-space, implies that, in the worst case, PRMs sampling requirements will grow exponentially with C-space dimension.

The above observations and the existence of new techniques from algebraic topology are the primary motivators of the work reported here and in the authors' previous papers [14, 9]. In [9], a solution to the path planning problem for planar 2R-manipulator among a finite number of point obstacles

[3] "Completeness" implies that if a path exists, one will be found, and if one does not exist, this fact will be reported. It also implies that the algorithm will terminate in finite time.

was given. Through the analysis of the set of singular configurations (those for which the chain intersects itself or a point obstacle), C-free was found to form parallel component sheaves locally. A global cell decomposition of C-free was then accomplished by identifying all bifurcations of local component sheaves. Under general-position assumptions, the exact number of components of C-free was determined (this number is an upper bound when the assumptions and constraints are relaxed). The local component sheaf representation of C-free allowed us to efficiently answer the existence question (*i.e.,* Are two given collision-free configurations in the same component of C-free?). Most importantly, the analysis also dictated the design of exact, complete, path generation algorithms.

The goal of this paper is to extend the results obtained for 2R-manipulators to the case of 3R-manipulators in the plane.

3 Basic notation and terminology

Let $\{\phi_1, \phi_2, \phi_3\}$ be the joint angles of a 3-link serial manipulator (or simply, 3-chain) with link lengths $\{l_1, l_2, l_3\}$ as shown in Figure 1. The C-space of a 3-chain is the three-dimensional torus, $T^3 = S^1 \times S^1 \times S^1$, where ϕ_i is the coordinate on the i^{th} circle, for $i = 1, 2, 3$. Consequently, a three-dimensional cube $[-\pi, \pi]^3$ with the three pairs of parallel boundary surfaces identified can be used to represent T^3. Next, suppose that there is a finite set $\mathcal{O} =$

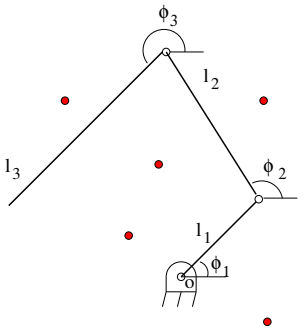

Fig. 1. A 3-chain among point obstacles (shown as small discs).

$\{p_1, p_2, \cdots, p_n\}$ of point obstacles. The C-obstacle is an arrangement of two-dimensional surfaces in T^3 (as shown in Figure 8).

The path planning problem is to find a collision-free motion of the manipulator transferring it between given initial and final postures. In other words, given $\phi_{\text{init}} = (\phi_1, \phi_2, \phi_3)_{\text{init}} \in$ C-free and $\phi_{\text{final}} = (\phi_1, \phi_2, \phi_3)_{\text{final}} \in$ C-free determine a continuous map $\tau \in [0, 1] \mapsto (\phi_1(\tau), \phi_2(\tau), \phi_3(\tau)) \in$ C-free such that $\phi(0) = \phi_{\text{init}}$ and $\phi(1) = \phi_{\text{final}}$.

Our analysis technique is recursive in the sense that when we study an m-chain, we use the results obtained for the proximal (m-1)-chain formed by removing one link from the distal end of the m-chain, *i.e.,* the end not pinned to the ground. This pattern of analysis will be seen in the review of the 2-chain case in the next section and in the subsequent analysis of the 3-chain case.

4 Review of the 2-chain case

Consider the 2-chain manipulator shown in Figure 2. C-free of the proximal 1-chain is a set of open intervals on the circle S^1 formed by removing the points, $\theta_{1,i}$, where link 1 intersects the i^{th} obstacle.[4] Fixing the first link and rotating the second link through a full circle gives a finite number of angles, $\theta_{2,i}(\phi_1)$, for which the second link intersects $\mathcal{O}$. These points are removed from the circle S^1 coordinatized by ϕ_2. To construct a representation of the C-free of the 2-chain, we start with the ϕ_1 circle with points removed. Then over each collision-free point, there is a finite number of disjoint open intervals of ϕ_2 that correspond to connected collision-free positions of link 2. The structure over each point is referred to as a *local component sheaf*.

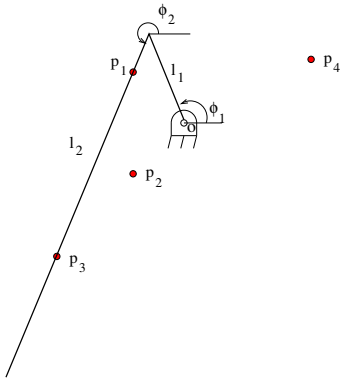

Fig. 2. A 2-chain that can reach all obstacles regardless of the angle of link 1.

This construction is illustrated in Figure 3 for the 2-chain shown in Figure 2. The angles $\theta_{1,1}$ and $\theta_{1,2}$ are values of ϕ_1 for which link 1 collides with $\mathcal{O}$. The "horizontal" *collision curves* above the ϕ_1-axis are curves corresponding to link 2 in contact with obstacles 1, 2, 3, and 4. For each point in the open interval, $(\theta_{1,1}, \theta_{1,2})$, the link 2 collision curves partition the ϕ_2 circle into a finite number of disjoint open intervals corresponding to collision-free configurations of link 2. Note that as ϕ_1 varies, the order of the collision curves above ϕ_1 changes at the points where they cross. These are the *critical points*

[4] This is at most n points, since n is the number of point obstacles.

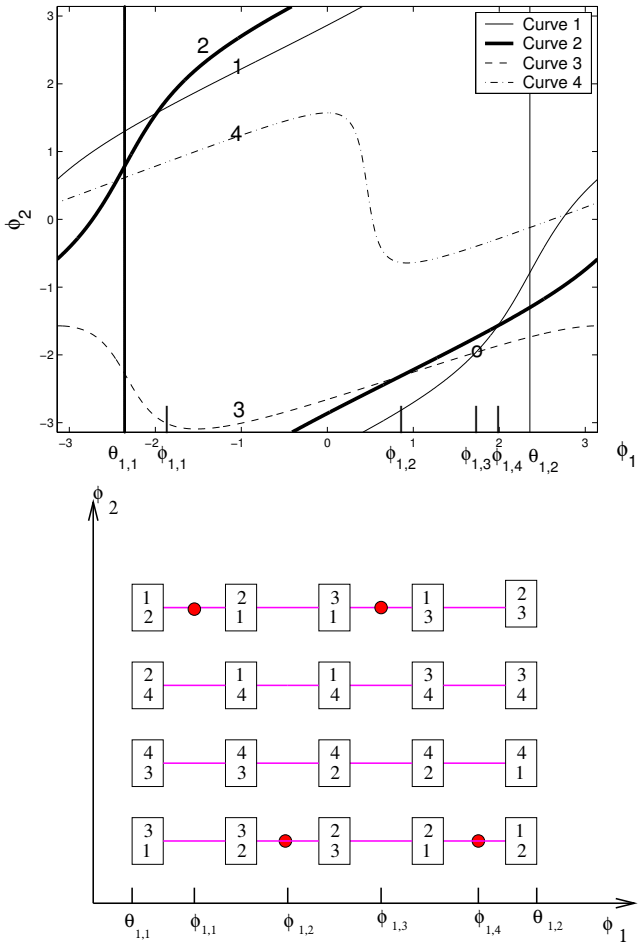

Fig. 3. Upper: C-space of 2-chain in Figure 2 showing all six collision curves (all are circles on the torus). Lower: Graph representing global structure of C-free over $(\theta_{1,1}, \theta_{1,2})$.

$\phi_{1,j}$ (where j ranges over an appropriate index set), when link 2 lies on a line containing two or more point obstacles.

For planning purposes, the free space over the open interval $(\theta_{1,1}, \theta_{1,2})$ can be represented as a graph, as shown in lower portion of Figure 3. A node (rectangle containing two curve indices) represents a portion of a cell of C-free bounded by the collision curves above and below and by the critical points of $\phi_{1,i}$ on the left and right. An arc connecting two nodes indicates that the nodes represent connected portions of a larger cell of C-free. A dot on the arc indicates that the corresponding free space chunks are not connected. Reversal of the label order corresponds to the crossing of two collision curves and so

the corresponding cells are not connected. Inspection of Figure 3 reveals 8 cells (recall that the top and bottom edges of the square are identified).

If link 2 is long enough to reach all obstacles regardless of the value of ϕ_1, then the "horizontal" collision curves will be closed as they are in Figure 3, and in this case the critical points are all of the type described above. However, if link 2 is not long enough, then for some values of ϕ_1, the second link will not be able to reach all obstacles. This case is illustrated on the left side of Figure 4, from which one can infer that for a set of values of ϕ_1, p_3 or p_4 cannot be reached by link 2. Thus there is a second type of critical point, which corresponds to the situation where the tip of the second link touches a point obstacle. In a neighborhood of such a critical point $\phi_{1,j}$, for ϕ_1 on one side of $\phi_{1,j}$ there are $\gamma \leq n$ open intervals, while on the other side there are strictly fewer than γ. The graph representation used above can be easily modified to handle the second type of critical point as shown on the right side of Figure 4. Finally, one can see that C-free has the maximum number of

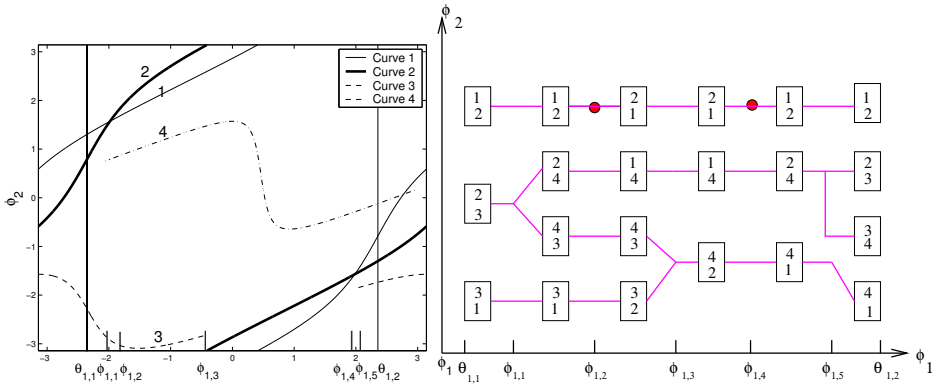

Fig. 4. Left: C-space of 2-chain with a shorter l_2 in Figure 2 showing collision curves, some of which are open. Right: Corresponding graph representing the global structure of C-free over ($\theta_{1,1}$, $\theta_{1,2}$).

components when all the curves are closed. In fact, this maximum number is the same for all generic arrangements of n obstacles, and is $2n^2 + n$ [9]. The number of components reduces monotonically as the length of link 2 reduces.

Since it is easy to determine cell membership of a configuration, graph search can be used to answer the path existence question. If a path is found to exist, it is easy to construct connected continuous curve segments through the cells to solve the path planning problem. All this is explained in detail in [9]. In addition, while we did not explicitly consider link-link collisions in the above discussion, one should note that the link-link collision curve is a single circle that is topologically equivalent to the link-obstacle collision curves, so the existence and planning problems can be solved without modifying the

analysis or logic above. Solutions to sample planning problems can be found in [9].

5 Overview of the analysis for the three-link case

As indicated above, the analysis of planar three-chains can be handled by observing that if we have a configuration of a three-chain that avoids the obstacle set, $\mathcal{O}$, then the proximal two-chain also avoids $\mathcal{O}$. Consequently, there is a projection of C-free of the three-chain to C-free of the proximal two-chain. Once more, if we are only concerned with avoiding collisions with $\mathcal{O}$, then over each point of C-free of the two-chain, the set of possible angles of the third link will be a circle with a finite number of points deleted, so this map is *onto*. Note that the situation is more complex if we also choose to avoid self-intersections since the intersections of the third link with the first is generally a three-dimensional subset of T^3. In any case, as we will see, over each point of the C-free of the two-chain, there will be a finite number of open intervals that represent the points for which link 3 avoids the obstacles and the other links. To determine the structure of C-free of the three-chain, in direct analogy to the approach taken for planar 2-chains, we locate the points in C-free of the proximal two-chain *where the number of intervals changes*.

We initially restrict our attention to the case where self-intersections are not considered. In this case the changes will occur over critical curves in C-free of the two-chain, analogous to the critical points identified in C-free of the proximal one-chain in the previous section. These critical curves will be of two kinds.

1. Type 1: Curves where there are γ open intervals above all points, (ϕ_1, ϕ_2), in a small neighborhood of the curve except for points on the curve, above which there are $\gamma-1$ (or fewer) intervals. These curves correspond to situations where link 3 can touch two (or more) point obstacles simultaneously.
2. Type 2: Curves where above all nearby points on one side of the curve there are γ open intervals, but only $\gamma - 1$ (or fewer) open intervals above nearby points on the other side. These curves arise from situations in which the tip of the three-chain touches a point obstacle.

Thus, to analyze the three-link case, one begins with the free space cells of the proximal two-chain and refines them by adding the critical curves. Recall that the critical points added to the free space cells (open intervals of the circle) of the proximal one-chain in the previous section did not change the topology of C-free of the one-chain. In Figure 3, ϕ_1 could still vary freely in the interval $(\theta_{1,i}, \theta_{1,i+1})$ across the critical points. Those points were only needed to understand the connectivity of free space "upstairs," *i.e.,* in the C-space of the two-chain. Similarly, in the three-link case, the critical curves running through the free space cells "downstairs" (in the C-space of the proximal two-chain) do not change the topology of those cells.

Figure 5 illustrates the refinement induced by a critical curve labelled "D." The graph representation below the plot and to the left is all that is needed to describe the free space of the proximal two-chain. However, in anticipation of adding the third link, we must include all critical curves such as D. These curves gives rise to additional "critical" points in the free space of the two-chain, and induces a refinement of the free space graph as shown below the plot and to the right. Note that nodes in the columns that contain D are connected by vertical arcs, because they do *not* disconnect the cells "downstairs."

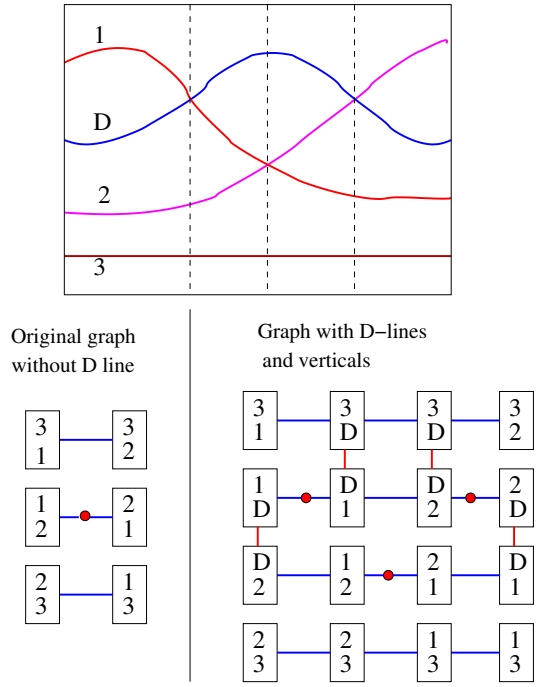

Fig. 5. Upper: Four cells of C-free generated by three point obstacles labelled "1," "2", and "3." Lower, left: The graph representation ignoring the critical curve D. Lower, right: The refined graph induced by the critical curve.

Figure 6 shows a rectangular free space cell "downstairs," crossed by a critical curve labelled "D". "Upstairs" there are the free space cells partitioned by four surfaces corresponding to the three-chain in contact with point obstacles 4, 5, 6, and 7. Two of the surfaces cross, at configurations where the three-chain simultaneously touches obstacles 4 and 5. The fact that this intersection separates the [4-5] cell from the [5-4] cell is the reason that the projection of the intersection curve is needed in the refinement of the free space of the proximal two-chain. This information is incorporated into the graph shown in the right portion of Figure 6 by growing the graph out of the

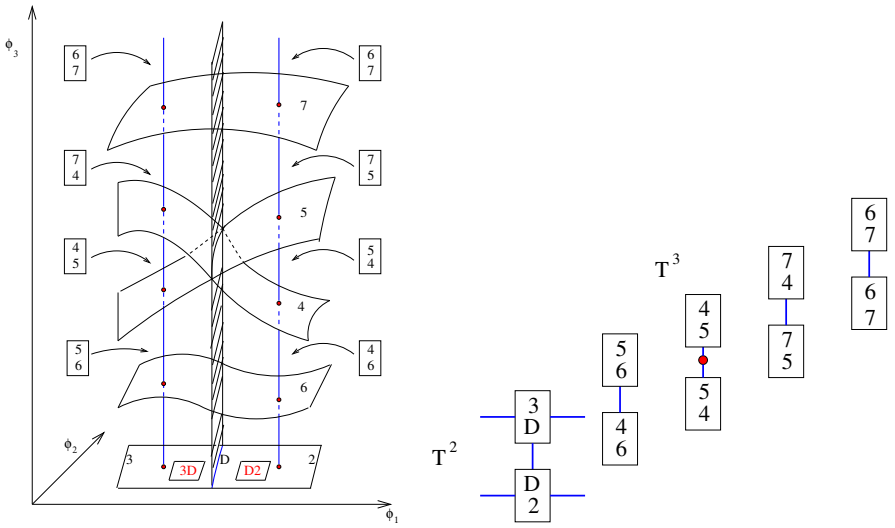

Fig. 6. Left: Component sheafs "above" two points in a cell of C-free of the proximal two-chain that are generated by adding a third link. Right: corresponding graph representing C-free for the 2-chain in T^2 ([3-D], [D-2]) and for the 3-chain in T^3 (the other 8 nodes corresponding to 5 components).

plane. The simple situation shown in the left portion of Figure 6, gives rise to four layers of the graph in the vertical direction - one for each surface. On the left is the free space cell [3-D,D-2] "downstairs." Above that are five free space cells "upstairs," [5-6,4-6], [4-5], [5-4], [7-4,7-5], and [6-7,6-7].

The discussion above shows the importance of understanding the subsets of the C-space of the three-chain where it intersects the obstruction set $\mathcal{O}$. We denote this intersection set Sing_2. We denote the subspace of configurations where the mechanism intersects itself Sing_1 and the union of these two spaces as

$$\text{Sing} = \text{Sing}_1 \cup \text{Sing}_2.$$

In the following section we analyze the set Sing_2. The analysis of Sing_1 will not be addressed here, interested readers can refer to our forthcoming technical report [10] for the details. However, we must emphasize here that Sing_1 for a three-chain has the same dimension as its C-space, while that for a two-chain has smaller dimension than its C-space.

6 Analysis of the set Sing_2

Let V_{p_i} be the collision surface which consists of all the configurations where the 3-chain intersects p_i. Under the assumptions that $\mathcal{O}$ is in general position and $l_2 > 2l_1$, $l_3 > 2(l_1 + l_2)$, V_{p_i} is the union of three surfaces, the first

a 2-torus, where ϕ_2 and ϕ_3 are arbitrary and l_1 intersects p_i, the second a 2-torus, where ϕ_3 is arbitrary and l_2 intersects p_i, while the third is also a 2-torus consisting of all configurations where p_i intersects l_3. In fact, for all $(\phi_1, \phi_2) \in T^2$, there is a unique angle ϕ_3 for the last joint such that link 3 collide with p_i. C-free will be $T^3 - \cup_i V_{p_i}$.

6.1 A Key Property of V_{p_i}

Let $C_{V_{p_i}}$ be the complement of V_{p_i} in T^3, *i.e.*, $C_{V_{p_i}} = T^3 - V_{p_i}$.

Proposition 1. *$C_{V_{p_i}}$ is the product of three open intervals. If we weaken our assumption on $\mathcal{O}$ so that $l_1 < |p_i| < l_2 - l_1$, then $C_{V_{p_i}}$ is the product of two open intervals and a circle. If $l_1 + l_2 < |p_i| < l_3 - (l_1 + l_2)$ then $C_{V_{p_i}}$ is the product of an open interval with two circles.*

Proof: We prove the first statement. The proofs for the second and third are similar. For the first statement, note that $|p_i| < l_1$. The projection of $C_{V_{p_i}}$ to the ϕ_1 axis will be the interval $S^1 - \{\theta_1\}$, where θ_1 is the angle of the first joint for which the first link lies on the line joining p_i to the origin. For each $\phi_1 \in S^1 - \{\theta_1\}$, there is one and only one configuration (ϕ_1, θ_2) at which the second link of the manipulator will collide with p_i. Note also that for all $(\phi_1, \phi_2) \in S^1 - \{\theta_1\} \times S^1 - \{\theta_2(\phi_1)\}$, there is again only one configuration $(\phi_1, \phi_2, \theta_3)$ at which the third link will collide with p_i. Therefore, the inverse image of ϕ_1 will be the product of two open interval $S^1 - \{\theta_2\} \times S^1 - \{\theta_3\}$. This decomposition is locally a product so the total space of $C_{V_{p_i}}$ fibers over the interval with fiber an open rectangle. Since any fibration over the interval is a product of the fiber with the interval, the proposition follows.

Remark 1. This result generalizes directly to m-R manipulators as long as for every configuration of the first $j-1$ joints, there is an angle for the j^{th} joint so that that link will pass through p_i, $j = 1, 2, \ldots$. The complement of $C_{V_{p_i}}$ on $T^m = S^1 \times \cdots \times S^1$ will be the direct product of m open intervals, and V_{p_i} will be the $m-1$-skeleton of T^m, the union of the m coordinate $m-1$ torii of T^m.

Once one has the V_{p_i}, in order to determine the entire structure of Sing_2 it is necessary to determine the intersections,

$$V_{p_{i_1}} \cap V_{p_{i_2}} \cap \ldots \cap V_{p_{i_r}}.$$

For reasonably general obstruction sets, $\mathcal{O}$, and lengths $l_1,\ l_2,\ l_3$, the intersections of 4 or more V_{p_i} will be empty, but it is easy to construct special sets $\mathcal{O}$ for any given 3R-manipulator where the intersections will be non-empty for much larger numbers of V_{p_i}.

Since any $\mathcal{O}$ and $\{l_1, l_2, l_3\}$ is arbitrarily close to a general $\mathcal{O}$, we make the assumption that four-fold intersections of the V_{p_i} are empty. In fact we can be more exact. We can assume, first,

- no three distinct points of $\mathcal{O}$ lie on a single line,
- no three lines, each through 2 distinct points of $\mathcal{O}$, intersect in a point,
- the first link does not collide with more than one point of $\mathcal{O}$ at a time, and
- by varying the lengths $l_1,\ l_2$, slightly, that the only configurations with three collision points will be isolated points in T^3 and will have the form $(1,1,1),\ (1,0,2)\ (0,2,1),\ (0,1,2)$, where the first number is the number of collisions with l_1, the second represents the number of collisions with l_2, and the third represents the number of collisions with l_3.

Remark 2. It is worth noting that the assumptions above imply that there will only be five types of 2-point collisions, having the forms $(1,1,0)$, $(1,0,1)$, $(0,1,1)$, $(0,2,0)$, $(0,0,2)$.

Let us now look at the intersection of V_{p_i} and V_{p_j} in more detail. A configuration that collides with both p_i and p_j can do so in two distinct ways. In the first way p_i collides with l_r and p_j collides with l_s where $s \neq r$. In the second way, l_r collides with both p_i and p_j.

We consider the case where $p_i \in l_1$ and $p_j \in l_3$. Since the requirement that $p_i \in l_1$ determines ϕ_1, we see that the initial point of l_2 is fixed and this piece of $V_{p_i} \cap V_{p_j}$ consists of a closed segment of the ϕ_2 circle. This segment will be the entire circle if $l_3 > l_2 + d$ where d is the distance from the initial point of l_2 to p_j. It will be empty if $d > l_3 + l_2$.

If $p_i \in l_1$ while $p_j \in l_2$, then both ϕ_1 and ϕ_2 are fixed provided $|p_i| \neq l_1$ while ϕ_3 is free, so this piece of the intersection is a circle.

The final piece of this type is where $p_i \in l_2$ and $p_j \in l_3$. In this case l_2 is constrained to lie in a region where its initial point lies on the circle of radius l_1 about the origin, $p_i \in l_2$ and the end-point lies in the closed disk of radius l_3 about p_j. The curve given by the end-point of l_2 under the constraint that the initial point of l_1 is fixed, and l_2 contains p_i is a simple closed curve coordinatized by either the entire l_1 circle, or an arc on it.

Next we consider the double point arcs, $p_i, p_j \in l_s$. We can assume that l_1 never intersects two of the obstruction points. If two obstruction points lie on l_2, then the end of l_1 must lie on the line connecting p_i, p_j, and both p_i, p_j must be on the same side of this point. If this happens, then ϕ_1 takes either one or two distinct values, and ϕ_2 is also fixed, but ϕ_3 is free, so we get either one or two circles. Finally, if p_i and p_j lie on l_3, then the end-point of the l_1, l_2, configuration must lie on the line connecting p_i, p_j, and on one side of this line only. The l_1, l_2 workspace is an annulus and various possibilities occur.

7 Determination of the Components for a Key Example

Assumption. 1 *As in the previous section we assume first that $\mathcal{O}$ and $\{l_1, l_2, l_3\}$ are in general position. We also make the following assumptions: $l_3 > 2(l_2 + l_1)$, $l_2 > 2l_1 > 0$, and $|p_i| < l_1$ for each $p_i \in \mathcal{O}$.*

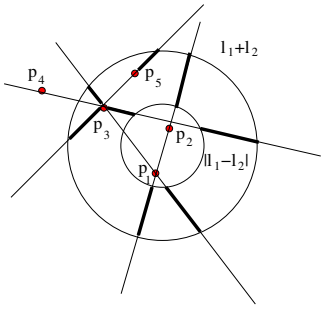

Fig. 7. The locations for the end-point of link 2 from which two obstacles can be touched by link 3 are drawn as bold line segments interior to the annulus.

As we will see, this results in a situation where there are no type-2 curves in the C-space of the first two links. Also, all collision surfaces will be closed, and all the generic intersections between collision surfaces will be present. When the assumptions are weakened, the arrangement of surfaces becomes simpler. Some surfaces open up, others disappear, and the intersections may also disappear.

From Proposition 1, we see that each V_{p_i} is a copy of the 2-dimensional skeleton of T^3. It is the union of three tori, T^2. The intersection between each two of these tori is a circle, and that between all three is a point, the point corresponding to the configuration where each link collides with p_i.

When we restrict to the first two links and the same $\mathcal{O}$ we get the assumptions studied in [9] so that $T^2 - \text{Sing}_2$ is fully understood. Over each point of $T^2 - \text{Sing}_2$, and for each $p_i \in \mathcal{O}$, there is an angle ϕ_3 so that l_3 collides with p_i due to the conditions in Assumption 1. Thus, for almost all the points of $T^2 - \text{Sing}_2$, the inverse image in $T^3 - \text{Sing}_2$ consists of n open intervals where n is the number of points in $\mathcal{O}$. The points where there are $\leq n-1$ intervals are those where the tip of the proximal 2-chain lies on one of the lines through two distinct points of $\mathcal{O}$.

Since each $p_i \in \mathcal{O}$ satisfies the condition $|p_i| < l_1 < |l_2 - l_1|$ it follows that any point in the intersection of the workspace of the two-link configuration - the annulus with radii $l_2 - l_1$ and $l_1 + l_2$ - with a line through two points of $\mathcal{O}$ lies on the same side of both points, and each such intersection consists of two intervals, each with endpoints on the $l_2 - l_1$ and $l_1 + l_2$ circles corresponding to the two different orders for p_i and p_j on l_3. *The inverse image of each such interval is a circle in T^2 that can be parameterized by ϕ_1.* These are the two point curves D discussed in Section 4.

What is not determined by the general discussion in Section 5 is the number and disposition of the intersections of the D. Such intersections correspond to the isolated points of $T^2 - \text{Sing}_2$ where the inverse image consists of exactly $n-2$ open intervals, and correspond, on $T^3 - \text{Sing}_2$, with the intersections of two of the D. Let the number of such intersections be N. Since the line

through p_i and p_j intersects the line through p_i and p_k, $k \neq j$ at p_i, it follows that two such lines can intersect the proximal 2-chain only if $p_i,\ p_j$ is disjoint from p_k, p_l, so we have

$$0 \leq N \leq \frac{n(n-1)(n-2)(n-3)}{8}.$$

However, since the sets of two-point curves at an intersection point are indexed by disjoint pairs of points, it follows that the four V_{p_t} surfaces upstairs that intersect along copies of these curves upstairs do not all intersect, but rather intersect two at a time. Consequently, these intersections downstairs do not contribute to the component count upstairs.

The final thing to note is that the regions of the downstairs torus that are cut out by these assumptions are cells. Moreover, the two point curves, D, needed in T^2 to take account of the points where the number of intervals over a point of $T^2 - \mathrm{Sing}_2$ is not n cuts each cell into further cells since each double point curve is parameterized by ϕ_1 under Assumption 1.

From the remarks above we know that each component of $T^3 - \mathrm{Sing}_2$ is the product of a cell in $T^2 - \mathrm{Sing}_2$ with an interval, and is consequently a cell. (This is not something that generalizes to other configurations $\mathcal{O}$ and 3-chains that do not satisfy Assumption 1.) There are $n(n-1)$ of the D curves, and each breaks into $2n-1$ components when restricted to the inverse image of the free part of the proximal T^2 - $n-1$ for intersections of the form $\langle 0, 1, 2\rangle$ and n more for intersections of the form $\langle 1, 0, 2\rangle$. Thus there are

$$n(n(2n-1)) + n(n-1)(2n-1) = n(2n-1)^2$$

components in all for 3-chains and obstruction sets $\mathcal{O}$ that satisfy the conditions of Assumption 1.

8 Preliminary results

While there are a small number of technical details of our approach that still require rigorous proof, we have begun implementation of the basic method. The planning algorithm uses the algorithm developed for planar 2R-manipulators presented in [9] to obtain the necessary free space graph downstairs, then computes a refinement of the graph based on critical curves, and finally "lifts" the graph into the 3-torus. The path existence problem is then solved by determining the cell membership of the initial and final configurations. If a path exists, then the details of the structure of the cell components containing the points are used to construct a collision-free path. In the algorithm description below, $\tilde{\phi} = (\phi_1, \phi_2)$ denotes a sub-configuration of the proximal two-chain, obtained by ignoring the third link.

Path planning algorithm for planar three-chain

- Input: n point obstacles p_i, $i = 1, \cdots, n$ which are in generic positions, a planar 3-R manipulator with arbitrary link lengths, and two arbitrary configurations $\phi(0)$ and $\phi(T)$ representing, respectively, the initial and final configurations
- Output: (i) "False" if no path exists, "True" otherwise; (ii) If a path exists, then return a path connecting the initial and final configurations.

1. Call the two-chain planning algorithm given in [9] to determine whether $\tilde{\phi}(0)$ and $\tilde{\phi}(T)$ are in the same component of free space downstairs. If not, return "False." Otherwise a return the cell E that contains both $\tilde{\phi}(0)$ and $\tilde{\phi}(T)$.
2. Calculate the singular curves and build the spatial graph above the planar graph.
3. Identify the nodes corresponding to the initial and final configurations.
4. Search the graph to determine path existence (most cells will be represented by more than one node). If a path does not exist, return "False." Otherwise continue.
5. Using the path through the graph, construct a path downstairs between $\tilde{\phi}(0)$ and $\tilde{\phi}(T)$.
6. Lift the path into T^3.

Figure 8 shows the results of path planning for a three-chain with four point obstacles in the workspace. To facilitate viewing this path, the projection of this path to (ϕ_1, ϕ_2) plane as well as other curves are drawn in Figure 9.

9 Conclusions and future work

We have developed most of the basic theory and developed an initial algorithm for planning collision-free motions of planar 3-chains with point obstacles in its workspace. There are three main avenues for further research that we plan to explore. First, we plan to exploit the methods of topology and homology to develop a planning algorithm with provably minimal complexity. Second, these methods also indicate that it will be possible to determine path existence without analyzing the entire free space. Such a method would use a candidate path connecting the initial and final configurations, but this path need not be valid. The third avenue of interest is the extension to allow two-dimensional obstacles.

Acknowledgements

The authors would like to thank Srinivas Akella for his careful reading of an earlier draft of this paper and for his insightful comments. This work was partially supported by NSF grant 0139701 and Rensselaer Polytechnic Institute.

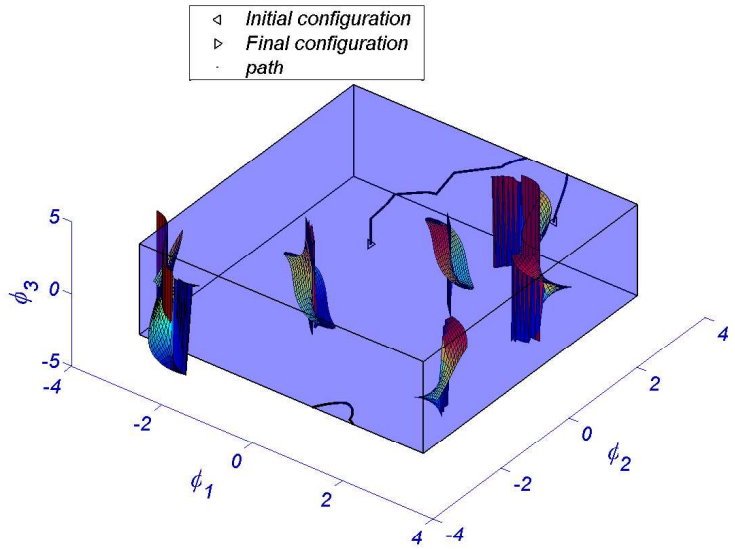

Fig. 8. C-space (T^3) with C-obstacle and a continuous path in C-free connecting the initial and final configurations. Note that due to the limitations of Matlab's "surf" function, a portion of the C-obstacle is plotted outside the cube.

References

1. J.F. Canny, *The complexity of robot motion planning.* Cambridge, MA: MIT Press, 1988.
2. P.C. Chen and Y.K. Hwang, *SANDROS: A dynamic graph search algorithm for motion planning.* IEEE Trans. on Robotics and Automation, **14**(3):390-403, 1998.
3. K.K. Gupta, *Fast collision avoidance for manipulator arms: A sequential search strategy.* IEEE Int'l. Conf. on Robotics and Automation, pp. 1724-1729, 1990.
4. D. Halperin, *On the complexity of a single cell in certain arrangements of surfaces related to motion planning.* Discrete and Comp. Geometry **11**:1-33, 1994.
5. Y. K. Hwang, N. Ahuja, *Gross motion planning - A survey.* ACM Computing Surveys **24**(3):219-291, 1992.
6. L.E. Kavraki, M.N. Kolountzakis, and J.C. Latombe, *Analysis of probabilistic roadmaps for path planning.* IEEE Trans. on Robotics and Automation, **14**(1):166-171, 1998.
7. L.E. Kavraki, P. Švestka, J.C. Latombe, and M.H. Overmars, *Probablistic roadmaps for path planning in high-dimensional configuration space.* IEEE Trans. on Robotics and Automation, **12**(4):566-580, 1996.
8. J.C. Latombe, *Robot motion panning.* Kluwer Academic Publishers, 1992.
9. G.F. Liu, J.C. Trinkle, R.J. Milgram, *Complete path planning for planar 2R-manipulators with point obstacles.* IEEE Int'l Conf. on Robotics and Automation, pp. 3263-3269, 2004.

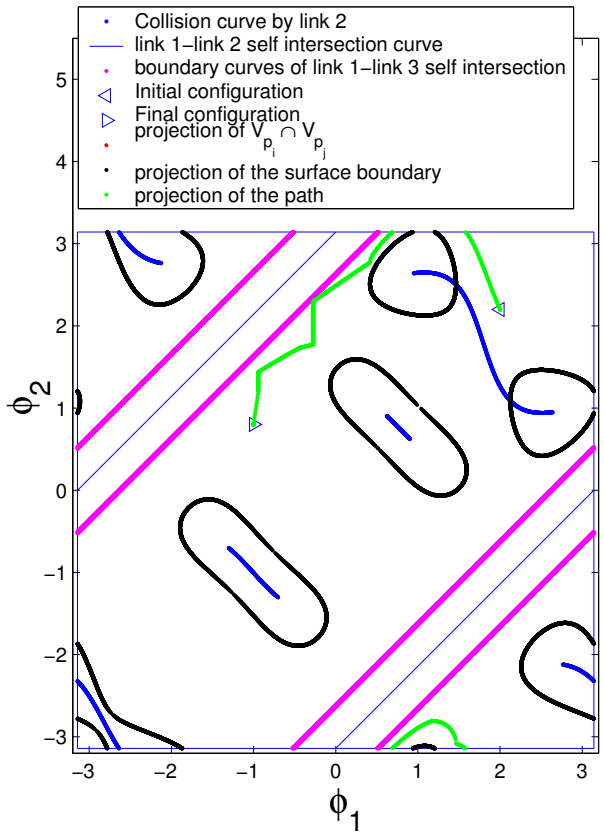

Fig. 9. The path and C-obstacle boundaries projected onto T^2.

10. G.F. Liu, J.C. Trinkle, R.J. Milgram, *Complete path planning for planar 3R-manipulators among point obstacles.* forthcoming tech. report, Dept. of Computer Science, Rensselaer Polytechnic Instiute, or through `www.cs.rpi.edu/~liugf/LTM-3R-planning.pdf`
11. T. Lozano-Pérez, *Spatial planning: A configuration space approach.* IEEE Transactions on Computers, **32**:108-120, 1983.
12. J. Schwartz, J. Hopcroft, and M. Sharir, *Planning, geometry, and complexity of robot motion.* Ablex, 1987.
13. J.T. Schwartz and M. Sharir, *On the piano movers II. General techniques for computing topological properties on real algebraic manifolds.* Adv. Appl. Math., **4**:298-351, 1983.
14. J.C. Trinkle and R.J. Milgram, *Complete path planning for closed kinematic chains with spherical joints.* Int'l Jrnl. of Robotics Research, **21**(9):773-789, 2002.
15. J.H. Yakey, S.M. LaValle, and L.E. Kavraki, *Randomized path planning for linkages with closed kinematic chains.* IEEE Trans. on Robotics and Automation, **17**(6):951-958, 2001.